

Article

Exploration of the DNA Photocleavage Activity of O-Halo-phenyl Carbamoyl Amidoximes: Studies of the UVA-Induced Effects on a Major Crop Pest, the Whitefly *Bemisia tabaci*[†]

Anastasios Panagopoulos¹, Konstantina Alipranti², Kyriaki Mylona² , Polinikis Paisidis³, Stergios Rizos³, Alexandros E. Koumbis³, Emmanouil Roditakis^{2,4}  and Konstantina C. Fylaktakidou^{1,3,4,*} 

¹ Laboratory of Organic, Bioorganic and Natural Product Chemistry, Molecular Biology and Genetics Department, Democritus University of Thrace, 68100 Alexandroupolis, Greece

² Department of Agriculture, School of Agricultural Sciences, Hellenic Mediterranean University, Gianni Kornarou, Estavromenos 1, 71410 Heraklion, Greece

³ Laboratory of Organic Chemistry, Chemistry Department, Aristotle University of Thessaloniki, 54124 Thessaloniki, Greece

⁴ Institute of Agri-Food and Life Sciences Agro-Health, Hellenic Mediterranean University Research Center, 71410 Heraklion, Greece

* Correspondence: kfylakta@chem.auth.gr

[†] This study is dedicated to the memory of D. N. Nicolaides, a passionate teacher, researcher, and mentor.

Abstract: The DNA photocleavage effect of halogenated O-carbamoyl derivatives of 4-MeO-benzamidoxime under UVB and UVA irradiation was studied in order to identify the nature, position, and number of halogens on the carbamoyl moiety that ensure photoactivity. F, Cl, and Br-phenyl carbamate esters (PCME) exhibited activity with the *p*-Cl-phenyl derivative to show excellent photocleavage against pBR322 plasmid DNA. *m*-Cl-PCME has diminished activity, whereas the presence of two halogen atoms reduced DNA photocleavage. The substitution on the benzamidoxime scaffold was irrelevant to the activity. The mechanism of action indicated function in the absence of oxygen, probably via radicals derived from the N-O bond homolysis of the carbamates and in air via hydroxyl radicals and partially singlet oxygen. The UVA-vis area of absorption of the nitro-benzamidoxime *p*-Cl-PCMEs allowed for the investigation of their potential efficacy as photopesticides under UVA irradiation against the whitefly *Bemisia tabaci*, a major pest of numerous crops. The *m*-nitro derivative exhibited a moderate specificity against the adult population. Nymphs were not affected. The compound was inactive in the dark. This result may allow for the development of lead compounds for the control of agricultural insect pests that can cause significant economic damage in crop production.

Keywords: amidoximes; DNA photocleavage; O-carbamoyl esters; N-O bond homolysis; *Bemisia tabaci*



Citation: Panagopoulos, A.; Alipranti, K.; Mylona, K.; Paisidis, P.; Rizos, S.; Koumbis, A.E.; Roditakis, E.; Fylaktakidou, K.C. Exploration of the DNA Photocleavage Activity of O-Halo-phenyl Carbamoyl Amidoximes: Studies of the UVA-Induced Effects on a Major Crop Pest, the Whitefly *Bemisia tabaci*. *DNA* **2023**, *3*, 85–100. <https://doi.org/10.3390/dna3020006>

Academic Editor: Amitava Adhikary

Received: 31 December 2022

Revised: 22 March 2023

Accepted: 27 March 2023

Published: 4 April 2023



Copyright: © 2023 by the authors. Licensee MDPI, Basel, Switzerland. This article is an open access article distributed under the terms and conditions of the Creative Commons Attribution (CC BY) license (<https://creativecommons.org/licenses/by/4.0/>).

1. Introduction

O-carbamoyl oximes, or otherwise oxime carbamates, are compounds that contain a $-\text{CO}-\text{N}(\text{R}^4\text{R}^5)$ group connected to the OH group of an oxime ($\text{R}^1\text{X}-\text{C}=\text{N}-\text{OH}$) (Figure 1(AI, AII)). X usually corresponds to H, an alkyl (or aryl), or an NR^2R^3 , namely, aldoximes, ketoximes, and amidoximes. All these derivatives contain a light-vulnerable N-O bond that dissociates under irradiation at a proper wavelength to provide, under a well-studied and known photochemistry, two radical residues: $[\text{R}^1\text{X}-\text{C}=\text{N}\cdot]$ and $[\text{R}^4\text{R}^5\text{N}-\text{CO}-\text{O}\cdot]$ (Figure 1(AIIa and AIIb), respectively). The fast decarboxylation of the carbamoyloxyl group allows for the generation of nitrogen-centered radicals (IIc), categorizing this class of compounds as photoreactive photobase generators (PBGs) [1,2]. PBGs have many applications in material and polymer chemistry. Representatively, thioxanthone amidines [3,4], *o*-nitrobenzyl based

tetramethylguanidines [5], simple carbamates [6], and *trans*-*o*-coumaric acid [7] find uses as UVA and visible light polymer photoinitiators in coatings, photoresists, etc. [8]. The same applies for oxime carboxylates and sulphonates [2,8–10], which on the other hand, act as photoacid generators releasing, upon irradiation, oxygen-centered radicals. In general, oximes are considered as functional molecules that provide nitrogen, oxygen, and carbon radicals [11] with interesting synthetic applications [10,12,13].

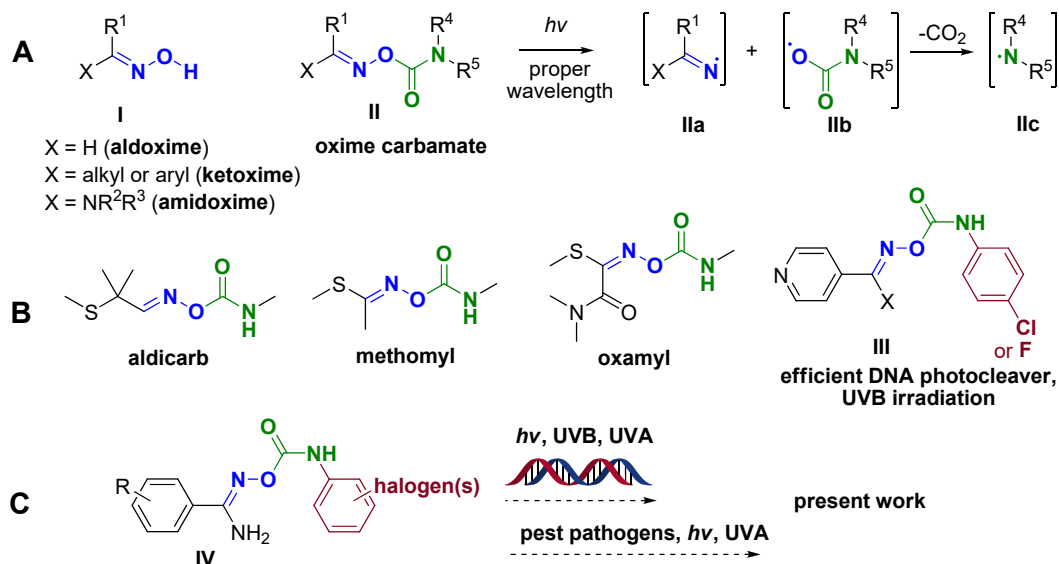


Figure 1. (A) Chemical structure of oximes (I) and their carbamate derivatives (II). Photochemical N-O homolysis of carbamates (II) that generate two nitrogen-centered radicals (IIa,IIc). (B) Chemical structures of commercially available oxime carbamates used as pesticides. (C) Present work.

O-carbamoyl oximes exhibit diverse biological activities. Benzoxazole and benzothiazole oxime carbamates were found to be active against *Mycobacterium tuberculosis* via a novel mode of action [14], benzoxadiazoles and analogs showed activity against *Leishmania donovani* [15], and some simple aromatic ones exhibited insecticidal activity against *Heliothis armigera* and *Plutella xylostella* [16]. Additionally, carbamates consist of a class of pesticides with widespread use that seem to decompose easier compared with other pesticides [17]. Pesticides that contain an oxime carbamate fragment, such as aldicarb, methomyl, and oxamyl (Figure 1B), along with others, are available in the market for use as insecticides, herbicides, etc. in the agriculture and food supply industries, although several restrictions and adverse effects accompany their use [17–21].

Pest control has great economic and social interest due to the fact that pests and insects are blamed for annual damage to enormous quantities of human and livestock's edible materials. Photodynamic inactivation derived from photopesticides seems to be an eco-friendly next-generation tool for the development of new and non-toxic pesticides for the control of pests and insect vectors, alternative to the conventional marketed products. A limited number of photosensitizers have been investigated for such purposes, and the results were promising, as the compounds were able to reduce the population of various species of agricultural pests such as *Ceratitidis capitata*, *Bactocera oleae*, *Colletotrichum acutatum*, and *Botrytis cinerea* [22].

Natural or synthetic scaffolds that include classical photosensitizers, such as xanthenes, porphyrin, phenothiazine, phthalocyanine, and curcumin derivatives, have been investigated [22]. A recent publication on porphyrin revealed the inactivation of *Botrytis cinerea*, a necrotic plant fungus that causes gray mold disease in over 200 crops [23], whereas the role of the photoreceptors for UVA-visible light of plant microbiota that influence infectivity, reproductive trails, and growth patterns is of great interest [24]. The xanthenes family of photosensitizers was the first to be used, and as has been mentioned, halogen substituents

have positively affected their photodynamic effect, increasing the intersystem crossing (ISC) yield for the triplet state and the formation of singlet oxygen, with the parallel radical production due to bond homolysis between halogens and aromatic rings [25]. This phenomenon was found also in other cases for the halogen substituted arenes [26–28], exemplifying their probably positive influence in photoapplications.

All kinds of oxime carboxylates and sulfonates were found to be activated by light and to efficiently photocleave DNA, providing reactive radicals derived from their N-O bond homolysis [29–37]. Studies to date have shown that oxime carboxylates allow for photoreactivity when the carboxylate group is aromatic, whereas for the sulfonate ones, both the aryl and alkyl groups seemed to efficiently yield DNA photo-scissions. Very recently, the activity of oxime carbamates towards DNA exhibited an interesting selectivity, showing the N-O bond dissociation, only when arylcarbamoyl groups were loaded onto a fluorine or a chlorine in the *p*-position (Figure 1(BIII)) [38].

This high specificity that was also verified via computational studies has prompted us to expand the study and to investigate the possible role of the aromatic imino group (R with various electronic effects in different positions on the ring), and the role of the nature, number, and position of the halogen group(s), as well as their DNA photodisruption efficacy. The compounds were designed in a way to absorb light under UVA irradiation in order to extend the study to “more friendly” irradiation wavelengths than UVB, which also has, although much limited, applications in phototherapies [39–46], compared to UVA.

Finding carbamates that may be photoexcited and absorbed in the UVA area, a first preliminary approach to investigating qualitatively possible pesticidal activity (Figure 1C) against a major insect (*Bemisia tabaci*), has, thus, been attempted. *B. tabaci* (Genadius) Homoptera: Aleyrodidae) is one of the most devastating pests of numerous crops worldwide. Its small size, extreme pace of reproduction, large host range, induction of phytotoxic reactions, and virus transmission, in conjunction with the ability to adapt to various climatic conditions, make controlling the population of this pest difficult to achieve [47–49]. Furthermore, it has lately been evident that this organism has developed resistance to major chemical classes of insecticides [50]. In particular, high levels of resistance have been reported for numerous substances with different modes of action [51], including ketoenols, neonicotinoids, organophosphates, etc. [52–54]. Therefore, new active ingredients with novel modes of action are needed in order to overcome this resistance and to apply management programs to efficiently control *B. tabaci*.

2. Materials and Methods

All commercially available reagent-grade chemicals and solvents were used without further purification. pB322 supercoiled plasmid was purchased from New England Biolabs (Ipswich, MA, USA). UV–visible (UV–vis) spectra were recorded on a Hitachi U–2001 (Hitachi, Tokyo, Japan) dual beam UV–Vis spectrophotometer. NMR spectra were recorded on an Agilent 500/54 (Agilent Technologies, Santa Clara, CA, USA) (500 MHz and 125 MHz for ^1H and ^{13}C , respectively) spectrometer using CDCl_3 and/or $\text{DMSO}-d_6$ as a solvent. *J* values were reported in Hz. High-resolution mass spectra were measured with a Q–TOF (Time of Flight Mass Spectrometry) Maxis Impact (Bruker Daltonics, Bremen, Germany) with ESI source and U–HPLC Thermo Dionex UltiMate 3000 RSLC (ThermoFisher Scientific, Dreieich, Germany) pump and autosampler. N_2 was used as the collision gas, and electrospray ionization (ESI) was used for the MS experiments. The data acquisition was carried out with a data analysis from Bruker Daltonics (Bremen, Germany) (version 4.1). All samples containing the pBR322 plasmid were irradiated at pH 6.8 with Philips $2 \times 9\text{W}/01/2\text{P}$ UV–B narrowband lamps at 312 nm (Pila, Poland) and Philips $2 \times 9\text{W}/10/2\text{P}$ UV–A broad band lamps at 365 nm. All reactions were monitored on commercially available pre-coated TLC plates (layer thickness 0.25 mm) of Kieselgel 60 F₂₅₄ (Merck, Darmstadt, Germany). Melting points were measured on Gallenkamp MFB-595 (USA) melting point apparatuses and were used uncorrected. Calculations of yields were based on the amount of crystallized product collected.

2.1. Synthesis of Chemical Compounds

General method for the synthesis of amidoxime carbamates (16–29): Isocyanates **6–15** (1.1 mmol) were individually added in a solution of the corresponding **1, 2, 4, 5** [55], or **3** [56] (1 mmol) in chloroform (15 mL, 0.7 M) at 0 °C. The mixture was stirred for 30 min and then refluxed for 1–6 h. The reaction was monitored by TLC. After cooling the reaction mixture to room temperature, the solvent was removed in a rotary evaporator and the resulting solid was recrystallized to give the pure product. Only in the case of compound **18** was purification performed using column chromatography over a silica gel with hexanes (hex) and ethyl acetate (E.A.) as the eluents. (Copies of the NMR spectra and HRMS analysis of all compounds are found in the Supplementary Materials, Section S1A and S1B, respectively, and those of the UV-vis spectra are found in the Supplementary Materials, Section S2A, whereas representative UV-vis spectra of four compounds with increasing amounts of CT-DNA are found in Section S2B).

- (Z)-*N'*-(4-chlorophenylcarbamoyloxy)-4-nitrobenzimidamide (**16**): reflux: 1 h; orange amorphous solid; mp: 196–198 °C (E.A./EtOH); yield: 91%; ¹H-NMR (DMSO-*d*₆, 500 MHz) δ 9.58 (s, 1H, NH), 8.31 (d, *J* = 8.5 Hz, 2H), 8.10 (d, *J* = 8.3 Hz, 2H), 7.57 (d, *J* = 8.5, 2H), 7.38 (d, *J* = 8.4 Hz, 2H), 7.09 (brs, 2H, NH₂) ppm; ¹³C-NMR (DMSO-*d*₆, 125 MHz) δ 154.2, 152.3, 148.7, 137.5, 137.4, 128.7, 128.2, 126.7, 123.5, 120.7 ppm; HRMS(ESI) *m/z* [M+Na]⁺: C₁₄H₁₁ClN₄O₄Na⁺, calc: 357.0361; found: 357.0361.
- (Z)-*N'*-(4-chlorophenylcarbamoyloxy)-3-nitrobenzimidamide (**17**): reflux: 1 h; yellow amorphous solid; mp: 210–212 °C (E.A.); yield: 89%; ¹H-NMR (DMSO-*d*₆, 500 MHz) δ 9.62 (s, 1H, NH), 8.63 (s, 1H), 8.36 (d, *J* = 7.8 Hz, 1H), 8.27 (d, *J* = 7.6 Hz, 1H), 7.78 (t, *J* = 7.9 Hz, 1H), 7.56 (d, *J* = 8.5 Hz, 2H), 7.37 (d, *J* = 8.5 Hz, 2H), 7.11 (brs, 2H, NH₂) ppm; ¹³C-NMR (DMSO-*d*₆, 125 MHz) δ 154.1, 152.4, 147.8, 137.6, 133.2, 132.9, 130.2, 128.7, 126.7, 125.3, 121.6, 120.7 ppm; HRMS(ESI) *m/z* [M+Na]⁺: C₁₄H₁₁ClN₄O₄Na⁺, calc: 357.0361; found: 357.0366.
- (Z)-*N'*-(4-chlorophenylcarbamoyloxy)-2-nitrobenzimidamide (**18**): reflux: 1 h; beige amorphous solid; mp: 142–145 °C (E.A./hex); yield: 50%; ¹H-NMR (DMSO-*d*₆, 500 MHz) δ 9.41 (s, 1H, NH), 8.08 (d, *J* = 8 Hz, 1H), 7.84 (t, *J* = 7.5 Hz, 1H), 7.78–7.70 (m, 2H), 7.53 (d, *J* = 8.7 Hz, 2H), 7.35 (d, *J* = 8.7 Hz, 2H), 7.08 (brs, 2H, NH₂) ppm; ¹³C-NMR (DMSO-*d*₆, 125 MHz) δ 154.8, 152.2, 148.4, 137.6, 133.4, 131.4, 131.3, 128.6, 126.7, 126.5, 124.2, 120.4 ppm; HRMS(ESI) *m/z* [M+Na]⁺: C₁₄H₁₁ClN₄O₄Na⁺, calc: 357.0361; found: 357.0367.
- (Z)-2-nitro-*N'*-(4-nitrophenylcarbamoyloxy)benzimidamide (**19**): reflux: 1 h; yellow amorphous solid; mp: 142–145 °C (EtOH/THF); yield: 75%; ¹H-NMR (DMSO-*d*₆, 500 MHz) δ 10.14 (s, 1H, NH), 9.32 (s, 1H, NH), 9.00 (s, 1H, NH), 8.15 (d, *J* = 8.5 Hz, 2H), 8.13 (d, *J* = 8.3 Hz, 1H), 7.87–7.78 (m, 3H), 7.73 (dt, *J* = 8.2, 1.3 Hz, 1H), 7.67 (d, *J* = 7.5 Hz, 1H) ppm; ¹³C-NMR (DMSO-*d*₆, 125 MHz) δ 165.7, 162.3, 147.0, 146.9, 141.1, 133.9, 132.0, 130.7, 129.9, 125.0, 124.2, 117.7 ppm; HRMS(ESI) *m/z* [M+Na]⁺: C₁₄H₁₁N₅O₆Na⁺, calc: 368.0607; found: 368.0564.
- (Z)-*N'*-(4-methoxyphenylcarbamoyloxy)-2-nitrobenzimidamide (**20**): reflux: 1 h; pale yellow amorphous solid; mp: 129–131 °C (E.A./EtOH); yield: 82%; ¹H-NMR (DMSO-*d*₆, 500 MHz) δ 9.03 (s, 1H, NH), 8.08 (d, *J* = 8 Hz, 1H), 7.83 (t, *J* = 7.3 Hz, 1H), 7.79–7.70 (m, 2H), 7.39 (d, *J* = 8.9 Hz, 2H), 7.08 (brs, 2H, NH₂), 6.88 (d, *J* = 9.0 Hz, 2H), 3.71 (s, 3H) ppm; ¹³C-NMR (DMSO-*d*₆, 125 MHz) δ 155.2, 154.3, 152.6, 148.5, 133.4, 131.5, 131.4, 131.3, 126.8, 124.2, 120.7, 114.0, 55.2 ppm; HRMS(ESI) *m/z* [M+Na]⁺: C₁₅H₁₄N₄O₅Na⁺, calc: 353.0856; found: 353.0871.
- (Z)-*N'*-(4-chlorophenylcarbamoyloxy)benzimidamide (**21**): reflux: 1 h; White amorphous solid; mp: 155–156 °C (hex/E.A.); yield: 90%; ¹H-NMR (CDCl₃, 500 MHz) δ 8.67 (s, 1H, NH), 7.68 (d, *J* = 7.5 Hz, 2H), 7.54 (t, *J* = 7.3 Hz, 1H), 7.50–7.43 (m, 4H), 7.29 (d, *J* = 8.6 Hz, 2H), 5.34 (brs, 2H, NH₂) ppm; ¹³C-NMR (CDCl₃, 125 MHz) δ 154.8, 152.7, 136.0, 131.5, 130.9, 129.2, 129.2, 129.1, 126.7, 121.0 ppm; HRMS(ESI) *m/z* [M+Na]⁺: C₁₄H₁₂ClN₃O₂Na⁺, calc: 312.0510; found: 312.0510.

- (Z)-*N'*-(4-chlorophenylcarbamoyloxy)-4-methoxybenzimidamide (**22**): reflux: 1 h; White amorphous solid; mp: 175–177 °C (hex/E.A.); yield: 88%; ¹H–NMR (CDCl₃, 500 MHz) δ 8.68 (brs, 1H, NH), 7.62 (d, *J* = 8.7 Hz, 2H), 7.46 (d, *J* = 8.7 Hz, 2H), 7.29 (d, *J* = 8.7 Hz, 2H), 6.97 (d, *J* = 8.7 Hz, 2H), 5.27 (brs, 2H, NH₂), 3.86 (s, 3H) ppm; ¹³C–NMR (CDCl₃, 125 MHz) δ 162.2, 154.5, 152.8, 136.1, 129.2, 128.2, 123.0, 121.0, 114.4, 55.6 ppm; HRMS(ESI) *m/z* [M+Na]⁺: C₁₅H₁₄ClN₃O₃Na⁺, calc: 342.0616; found: 342.0613.
- (Z)-*N'*-(4-fluorophenylcarbamoyloxy)-4-methoxybenzimidamide (**23**): reflux: 3 h; White amorphous solid; mp: 179–181 °C (hex/E.A.); yield: 89%; ¹H–NMR (DMSO-*d*₆, 500 MHz) δ 9.04 (s, 1H, NH), 7.77 (d, *J* = 8.9 Hz, 2H), 7.55 (dd, *J* = 9.0, 5.0 Hz, 2H), 7.16 (t, *J* = 8.9 Hz, 2H), 6.99 (d, *J* = 8.9 Hz, 2H), 6.74 (brs, 2H, NH₂), 3.81 (s, 3H) ppm; ¹³C–NMR (DMSO-*d*₆, 125 MHz) δ 161.0, 158.0 (d, ¹*J*_{C-F} = 238 Hz), 155.2, 152.9, 134.9 (d, ⁴*J*_{C-F} = 2.5 Hz), 128.3, 123.4, 122.1 (d, ³*J*_{C-F} = 7.8 Hz), 115.3 (d, ²*J*_{C-F} = 28 Hz), 113.7, 55.4 ppm; HRMS(ESI) *m/z* [M+Na]⁺: C₁₅H₁₄FN₃O₃Na⁺, calc: 326.0917; found: 326.0910.
- (Z)-*N'*-(4-bromophenylcarbamoyloxy)-4-methoxybenzimidamide (**24**): reflux: 1 h; White amorphous solid; mp: 150–152 °C (hex/E.A.); yield: 80%; ¹H–NMR (CDCl₃, DMSO-*d*₆, calibration on CDCl₃, 500 MHz) δ 8.70 (s, 1H, NH), 7.58 (d, *J* = 8.7 Hz, 2H), 7.35 (s, 4H), 6.88 (d, *J* = 8.7 Hz, 2H), 5.63 (brs, 2H, NH₂), 3.78 (s, 3H) ppm; ¹³C–NMR (CDCl₃, DMSO-*d*₆, calibration on CDCl₃, 125 MHz) δ 161.8, 154.8, 152.7, 136.7, 131.8, 128.1, 123.0, 121.1, 116.34, 113.9, 55.4 ppm; HRMS(ESI) *m/z* [M+Na]⁺: C₁₅H₁₄BrN₃O₃Na⁺, calc: 386.0116; found: 386.0111.
- (Z)-*N'*-(4-iodophenylcarbamoyloxy)-4-methoxybenzimidamide (**25**): reflux: 2 h; pale white amorphous solid; mp: 180–182 °C (hex/E.A.); yield: 85%; ¹H–NMR (CDCl₃, 500 MHz) δ 8.67 (s, 1H, NH), 7.62 (d, *J* = 8.6 Hz, 2H), 7.61 (d, *J* = 8.6 Hz, 2H), 7.30 (d, *J* = 8.6 Hz, 2H), 6.97 (d, *J* = 8.7 Hz, 2H), 5.26 (brs, 2H, NH₂), 3.86 (s, 3H) ppm; ¹³C–NMR (CDCl₃, 125 MHz) δ 162.2, 154.5, 152.6, 138.1, 137.3, 128.2, 123.0, 121.6, 114.5, 87.2, 55.6 ppm; HRMS(ESI) *m/z* [M+Na]⁺: C₁₅H₁₄IN₃O₃Na⁺, calc: 433.9972; found: 433.9970.
- (Z)-*N'*-(3-chlorophenylcarbamoyloxy)-4-methoxybenzimidamide (**26**): reflux: 3 h; White amorphous solid; mp: 162–165 °C (E.A./hex); yield: 90%; ¹H–NMR (CDCl₃, DMSO-*d*₆, calibration on CDCl₃, 500 MHz) δ 8.73 (s, 1H, NH), 7.41 (d, *J* = 8.5 Hz, 2H), 7.37 (s, 1H), 7.07 (d, *J* = 8.2 Hz, 1H), 6.94 (t, *J* = 8.0 Hz, 1H), 6.73 (d, *J* = 8.0 Hz, 1H), 6.64 (d, *J* = 8.5 Hz, 2H), 5.85 (brs, 2H, NH₂), 3.54 (s, 3H) ppm; ¹³C–NMR (CDCl₃, DMSO-*d*₆, calibration on CDCl₃, 125 MHz) δ 161.0, 154.6, 152.1, 138.7, 133.7, 129.4, 127.8, 122.8, 122.6, 118.6, 116.9, 113.3, 54.8 ppm; HRMS(ESI) *m/z* [M+Na]⁺: C₁₅H₁₄ClN₃O₃Na⁺, calc: 342.0616; found: 342.0621.
- (Z)-*N'*-(2-chlorophenylcarbamoyloxy)-4-methoxybenzimidamide (**27**): reflux: 6 h; White amorphous solid; mp: 133–135 °C (E.A./hex); yield: 82%; ¹H–NMR (CDCl₃, 500 MHz) δ 9.47 (s, 1H, NH), 8.30 (d, *J* = 8.2 Hz, 1H), 7.66 (d, *J* = 8.4 Hz, 2H), 7.38 (d, *J* = 8.0 Hz, 1H), 7.30 (t, *J* = 7.6 Hz, 1H), 7.03 (t, *J* = 7.6 Hz, 1H), 6.97 (d, *J* = 8.5 Hz, 2H), 5.29 (brs, 2H, NH₂), 3.85 (s, 3H) ppm; ¹³C–NMR (CDCl₃, 125 MHz) δ 162.1, 154.1, 152.6, 134.6, 129.2, 127.9, 127.9, 124.2, 123.2, 122.8, 120.5, 114.4, 55.5 ppm; HRMS(ESI) *m/z* [M+Na]⁺: C₁₅H₁₄ClN₃O₃Na⁺, calc: 342.0616; found: 342.0619.
- (Z)-*N'*-(((3,4-dichlorophenyl)carbamoyl)oxy)-4-methoxybenzimidamide (**28**): reflux: 3 h; White amorphous solid; mp: 153–155 °C (E.A./hex); yield: 80%; ¹H–NMR (CDCl₃, 500 MHz) δ 8.72 (s, 1H, NH), 7.72 (s, 1H), 7.61 (d, *J* = 8.7 Hz, 2H), 7.37 (brs, 2H), 6.97 (d, *J* = 8.7 Hz, 2H), 5.23 (brs, 2H, NH₂), 3.86 (s, 3H) ppm; ¹³C–NMR (CDCl₃, 125 MHz) δ 162.2, 154.7, 152.5, 137.1, 133.0, 130.7, 128.2, 127.3, 122.8, 121.3, 118.9, 114.5, 55.6 ppm; HRMS(ESI) *m/z* [M+Na]⁺: C₁₅H₁₃Cl₂N₃O₃Na⁺, calc: 376.0226; found: 376.0223.
- (Z)-*N'*-(2,4-dichlorophenylcarbamoyloxy)-4-methoxybenzimidamide (**29**): reflux: 3 h; White amorphous solid; mp: 154–157 °C (E.A./hex); yield: 79%; ¹H–NMR (CDCl₃, 500 MHz) δ 9.40 (s, 1H, NH), 8.15 (d, *J* = 9.0 Hz, 1H), 7.70 (d, *J* = 8.9 Hz, 2H), 7.48

(d, $J = 2.2$ Hz, 1H), 7.31 (dd, $J = 8.9, 2.2$ Hz, 1H), 6.94 (d, $J = 8.8$ Hz, 2H), 6.85 (brs, 2H, NH₂), 3.79 (s, 3H) ppm; ¹³C-NMR (CDCl₃, 125 MHz) δ 161.0, 154.7, 151.8, 133.5, 128.3, 127.8, 127.5, 127.4, 123.3, 122.7, 121.2, 113.5, 55.0 ppm; HRMS(ESI) m/z [M+Na]⁺: C₁₅H₁₃Cl₂N₃O₃Na⁺, calc: 376.0226; found: 376.0224.

Synthesis of (E)-1-(4-chlorophenyl)-2-(1-(4-nitrophenyl)ethylidene)hydrazine (32) [57]: 4-chlorophenylhydrazine hydrochloride **31** (179 mg, 1 mmol) was added in a mixture of ethanol (15 mL) and NaHCO₃ (138 mg, 1 mmol) at 0 °C and stirred for 5 min. Then, 4-nitroacetophenone **30** (165 mg, 1 mmol) and a few drops of acetic acid were added. After stirring the mixture for 1 h at the same temperature, the reaction mixture was heated at reflux for 1 h. Upon cooling, the formed precipitate was collected and recrystallized. Dark red amorphous solid; mp: 168–170 °C (E.A./EtOH); yield: 89%; ¹H-NMR (DMSO-*d*₆, 500 MHz) δ 9.81 (s, 1H, NH), 8.21 (d, $J = 8.7$ Hz, 2H), 8.02 (d, $J = 8.7$ Hz, 2H), 7.30 (s, 4H), 2.30 (s, 3H) ppm; ¹³C-NMR (DMSO-*d*₆, 125 MHz) δ 146.2, 145.3, 144.3, 139.0, 128.8, 125.9, 123.6, 123.2, 114.7, 12.7 ppm; HRMS(ESI) m/z [M+Na]⁺: C₁₄H₁₂ClN₃O₂Na⁺, calc: 312.0516; found: 312.0514.

2.2. Supercoiled Circular pB322 DNA Photo-Cleavage Experiments

The compounds were irradiated at various concentrations with UV-visible light (312 nm, narrow band—18 W; 365 nm, broad band—18 W; or visible light 400–700 nm—18W) under aerobic conditions at room temperature for 30 min and at a 15 cm distance (312 nm), or for 2 h and at a 10 cm distance (365 nm or visible light). The conditions of the gel preparation and quantification of the DNA-cleaving activity have been provided earlier [35]. Briefly, the reaction mixtures (20 μ L) containing the supercoiled circular pB322 plasmid DNA stock solution (Form I, 500 ng), compounds, and Tris buffer (25 μ M, pH 6.8) in Pyrex vials were incubated for 30 min at 37 °C, centrifuged, and then irradiated.

2.3. Toxicological Bioassays of *Bemisia tabaci*

The *B. tabaci* population tested in this study was collected in 2021 from a greenhouse of melon crops in the region of Tympaki, Crete (35°5′12.78″ N, 24°45′7.86″ E), and was provided with the code name TYM 21-3, which will be used hereafter. The population was maintained in a laboratory culture on cotton plants under controlled environmental conditions (24 \pm 1 °C, 16 hL: 8h D).

The toxicological bioassays used here were based on approved IRAC method protocols (<https://irac-online.org/> accessed on 30 March 2023). More specifically, the bioassay methods IRAC 015 and IRAC 016 were employed for testing the lethal effects of compound **17** on *B. tabaci* adults and nymphs (L2 instar), respectively [58,59]. The substance was used at a concentration of 400 mgL⁻¹. In order to perform the toxicological assays, the compound was dissolved in dimethylformamide (DMF) and an emulsifier (EM) in a ratio of 3:1. The mixture was subsequently dissolved in water, providing a homogenous emulsion.

2.3.1. Bioassays of *Bemisia tabaci*

The leaf dip bioassay method on whitefly nymphs was performed based on protocol IRAC016 described in Bielza et al. [53]. Briefly, two cotton plants with two true leaves were used during the experimental process. Approximately, 50 adult whiteflies from the TYM 21-3 were caged on individual cotton leaves in small clip cages for a 24 h oviposition period to allow for synchronization of the developing nymphal stages. After oviposition, the adults were removed. Each treatment was performed in four replicates. The tested plants were maintained at 25 (\pm 2) °C, 60% RH. Upon a period of nine days, when the majority of the nymphs had reached the second instar (L2), the leaves were immersed in an emulsion of 400 mgL⁻¹ of **17** for 10 s. For the control, the leaves were immersed in an emulsion that contained only the solvents DMF and EM. Finally, the mortality was assessed approximately after 15 days, when the nymphs reached the final instars on the infested leaves. An insect was considered dead if the nymphs were dried-out or/and did not develop further than the initial second instar.

Concerning the adults' tests, aqueous emulsions of compound **17** were used in a leaf dip bioassay protocol (IRAC015) previously described by Roditakis et al. [50]. Briefly, three cotton leaf discs were cut to fit 39 mm diameter Petri dishes per treatment. The leaves were immersed in 400 mgL⁻¹ of **17** for 5 s. For the control, the leaves were immersed in an emulsion that contained only the solvents DMF and EM. Treated leaf discs were allowed to dry and placed with the abaxial surface in Petri dishes embedded with a thin sterile water agar layer (20 g L⁻¹). Two ventilation holes covered with thin meshes had been opened on the side walls of the dish to allow for adequate ventilation. Then, whiteflies adults were restrained using carbon dioxide, and 25 females were placed on each leaf dish. Handling mortality was estimated within 1 h. The corrected mortality was assessed after 72 h. An insect was considered dead if no movement was observed after disturbance of the insect with a fine brush.

The aforementioned bioassays were conducted with (UVA 365 nm, 18W, 24 h exposure) and without UVA irradiation (24 h in the dark) in order to evaluate the effect of UVA irradiation on compound's lethal activity on whiteflies. Subsequently, the bioassay dishes were transferred under typical environmental conditions (24 ± 1 °C, 16 hL: 8 h D) up to the time point that insect mortality was evaluated, as previously described.

2.3.2. Data Analysis and Statistics

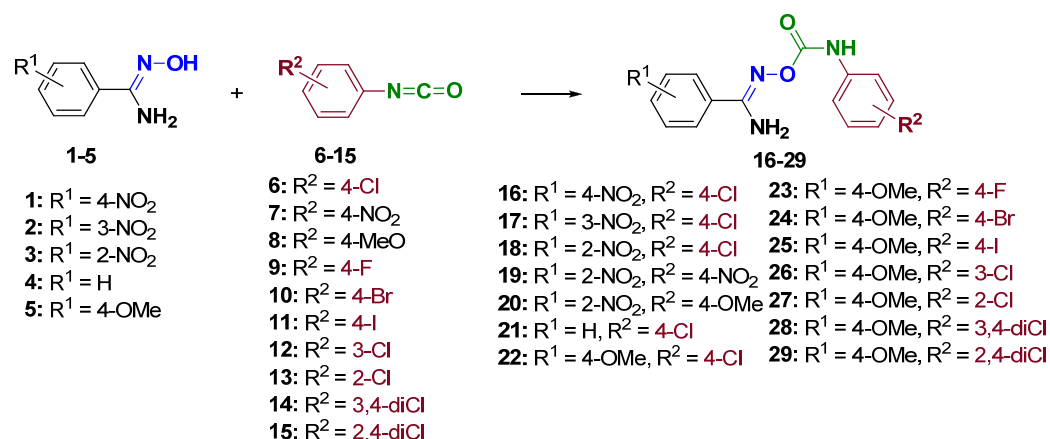
Mortality % was corrected for control mortality using Abbott's formula [60]. The analyses were performed using IBM SPSS statistics version 28.0. The corrected mortality between UVA and no UVA treatments were compared with one-way analyses of variance (ANOVA). Before statistical analyses were performed, homogeneity and the normality of error of variances were evaluated for all data groups.

3. Results and Discussion

3.1. Chemistry

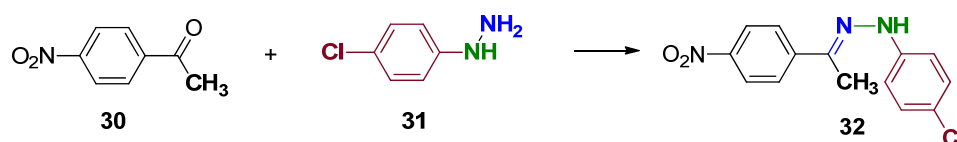
A selection of appropriate parent aromatic amidoximes **1**, **2**, **4**, **5** [55], and **3** [56] bearing substituents of the electron donating and withdrawing effects were reacted initially with commercially available *p*-Cl-phenylisocyanate **6** in chloroform reflux for 1–6 h to afford good to excellent yields of carbamoyl derivatives diversified on the aromatic ring of the amidoxime moiety (Scheme 1, **16–18** and **21–22**). In our previous work on the DNA photocleavage activity of oxime carbamates, along with the experimental proof, computational calculations showed that only a *p*-Cl (compared with a *p*-NO₂)-substituted phenylcarbamoyl conjugate had the capacity to react under light, giving a populated excitation triplet state, whereas other moieties such as *p*-MeO-phenyl, *p*-NO₂-phenyl, phenyl, or benzyl were found to become photo-reacting towards DNA only after the addition of a triplet state activator [38]. In order to obtain another experimental proof for this concept, *o*-nitrophenyl amidoxime (**3**) was reacted with commercially available *p*-NO₂-phenyl (**7**) and *p*-MeO-phenyl isocyanate (**8**), furnishing two additional carbamate esters (**19,20**).

After performing DNA photocleavage experiments at 312 nm, all derivatives, except **19** and **20**, were found to be very active, a result that verified again the findings of previous studies. The correlation of the DNA-photocleaving ability to the existence of a halogenated carbamoyl motif was further investigated. Taking into account the very good photocleaving activity of the compounds at 312 nm, the MeO derivative **22** was chosen as a lead for a second stage of studies, which were designed in order to identify the effect of the nature, the number, and the position of halogens on the carbamoyl group. Thus, along with the *p*-Cl-phenyl conjugate, the *p*-F; *p*-Br; *p*-I; *m*-Cl; *o*-Cl; 3,4-di-Cl; and finally, 2,4-di-Cl-phenyl derivatives were prepared. Under similar reaction conditions, compounds **23–29** were uneventfully obtained in good to excellent yields (Scheme 1).



Scheme 1. Synthesis of carbamates: 1/1.1 equivalents of amidoximes and isocyanate esters, respectively, refluxed in CHCl₃ for 1–6 h.

All nitro-phenyl amidoxime carbamates (16–18) were found to absorb light in the UVA area. Therefore, the opportunity to compare their reactivity to a hydrazone derivative lacking the –O-CO- linker of the carbamates (Scheme 2 compound 32 [57]) was important for the completion of the comparative studies.



Scheme 2. Synthesis of hydrazone 32.

Besides 32 [57], all compounds are new and were fully characterized. For 16–29, a single geometric isomer (*Z*) was isolated in all cases. Moreover, as for amidoxime carbamates with quite similar structures [38], the oxyimino moiety was being identified by the existence of a broad singlet peak, integrated for two protons, at 5.2–7.7 ppm (NH₂). The singlet sharp peak in the area of 8.7–10.1 ppm in the ¹H-NMR spectrum corresponds to the NH moiety of the carbamate group.

3.2. DNA Photocleavage Experiments

Plasmid DNA exists in three conformations. The first one, the supercoiled form (called Form I) is the basis for the calculations of DNA damage. When it is nicked at a single strand (ss), it gives the relaxed or open circular form (Form II). For the same size, the supercoiled DNA runs faster in gel electrophoresis than relaxed DNA and provides a second discrete band. When both strands are cut, this double strand (ds) damage provides the linear form of the plasmid that sustains less friction than relaxed circular DNA, but more than supercoiled DNA. By staining the irradiated DNA with EB, the latter band is found in between Form I and Form II and is called Form III. All those bands can be measured based on the control plasmid DNA and give the % ss and % ds DNA damage.

Before irradiation, all compounds were incubated with plasmid DNA pBR322 for 30 min at 37 °C. Compared with compound 18, negligible activity has been shown by the *p*-NO₂-Ph and *p*-OMe-Ph carbamates, 19 and 20, respectively, at 500 μM concentration and at 312 nm irradiation (Supplementary Materials, Figure S3A), a fact that verifies the necessity of a halogen atom on the carbamate moiety. To go further into these studies, the concentration dependence of the DNA photocleavage has been studied for phenyl amidoximes bearing (i) an electron donor group (OMe), (ii) no substituent, and (iii) electron withdrawing groups (NO₂) (i) 22, (ii) 21, and (iii) 16 and 18). Thus, those derivatives have been exposed to UVB irradiation at concentrations of 1, 50, and 100 μM. As it can be seen, a concentration of 50 μM was already sufficient for effective photocleavage (Figure 2).

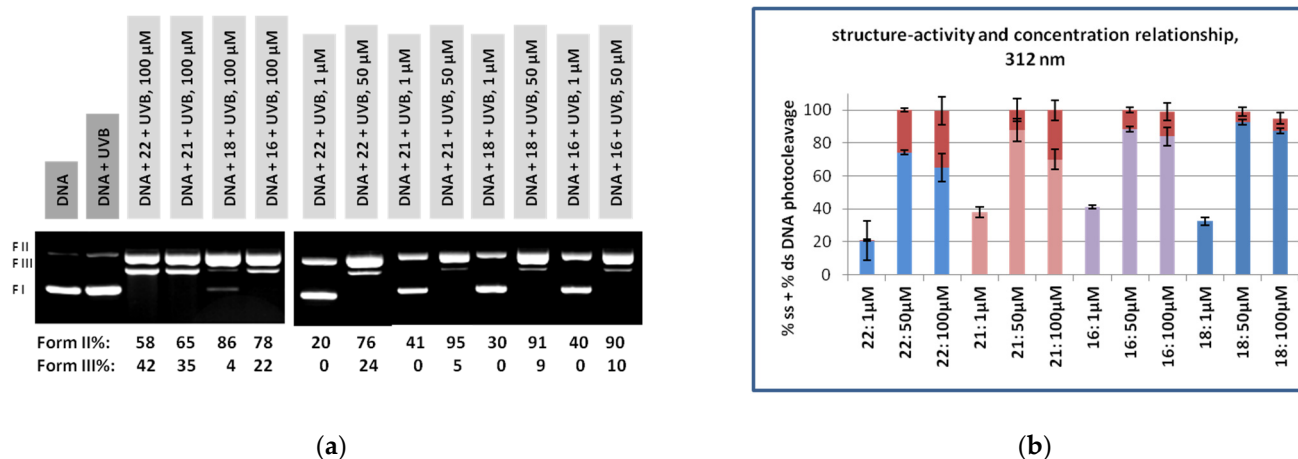


Figure 2. (a) Gel electrophoresis image depicting one experimental picture for the DNA photocleavage caused by selected amidoxime *p*-Cl-Ph carbamates **16**, **18**, **21**, and **22** at concentrations 1, 50, and 100 μM, 312 nm (F I: Form I; F II: Form II; F III: Form III); (Form II%: % ss; Form III%: % ds); (b) plots that depict all values derived from all (at least two) experiments for the same compounds. For each compound for the three concentrations the same color has been chosen (for example: blue for the % ss damage caused by compound **22**; For all compounds on the top of % ss damage the % ds damage is found in red color).

This study on the concentration/DNA photocleavage dependence for compound **22** indicated a progressive increase in the double strand photocleavage with concentration. About 50% of the plasmid was found to be cleaved between 1 and 10 μM (Supplementary Materials, Figure S3B). All four tested amidoximes seemed to be good candidates as substrates for the study of carbamates and the role of the halogens on DNA photocleavage. There was no specific reason to choose one derivative over the other, and thus, the MeO-Ph-amidoxime scaffold was, finally, chosen.

Therefore, derivatives **23–25** were exposed to UVB irradiation under the same conditions applied to **22**. It is obvious from the results (Figure 3) that the *p*-F, *p*-Cl, and *p*-Br-Ph conjugates yield to an extensive DNA photocleavage, which at 100 μM, has the ability to cause ss as well as ds damages. The best activity was observed for the *p*-Cl derivative (**22**), and the worst was observed for the *p*-I-Ph one (**25**). Finding chlorine as the halogen atom with the best activity, another set of derivatives (**26–29**) have been designed, synthesized, and exposed to UVB irradiation. Changing the position of the chlorine atom from *p*- to *m*- (**26**) led to a dramatic drop in activity. However, a small percentage of activity was preserved when comparing the *p*- to *o*-substituted analogue (**27**).

As for the bis-Cl substituted compounds, the 3,4-di-Cl (**28**) and 2,4-di-Cl-Ph (**29**) derivatives, the second chlorine atom at the *p*-position (**28**) increased the activity compared with the mono *m*-derivative **26**; nevertheless, the existence of a chlorine atom on the *m*-position seemed to be crucial for activity loss. On the other hand, two chlorine atoms at the *o*- and *p*-positions (**29**) showed activity in between the *o*- and *p*-derivatives, **27** and **22**, respectively; nevertheless, the superiority of compound **22** among all derivatives was more than obvious (Figure 3). All these model compounds were inactive in the dark (Supplementary Materials, Figure S3C).

The mechanism of action has been studied for derivatives **21** and **22** (100 μM concentration) in the absence of oxygen, as well as in air with a variety of radical and singlet oxygen scavengers. Both compounds showed similar activities that involved functioning under argon, which means that the N-O bond homolysis allows the oxime carbamates to create their nitrogen centered radicals [38] (Figure 4).

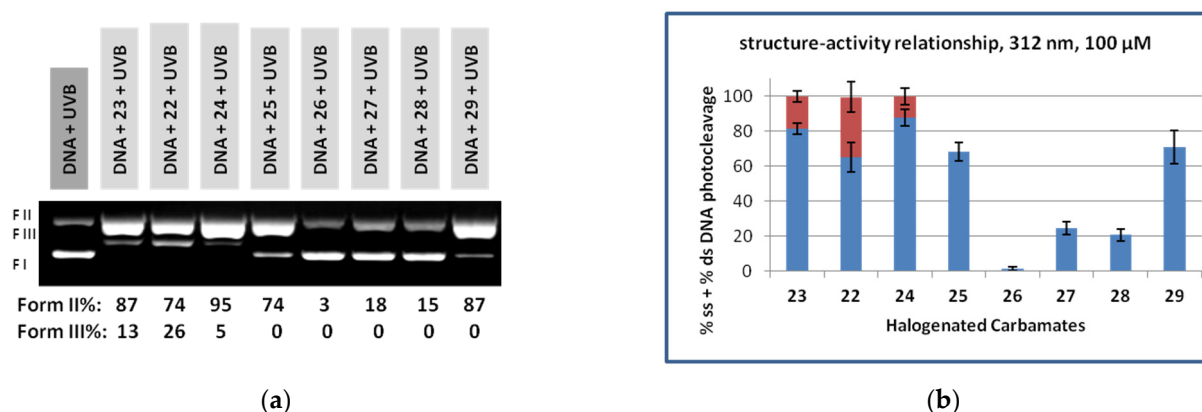


Figure 3. (a) Gel electrophoresis image depicting one experimental picture for the DNA photocleavage caused by all methoxy-amidoxime halogenated carbamate derivatives **22–29** at concentration 100 μ M and 312 nm irradiation (F I: Form I; F II: Form II; F III: Form III); (Form II%: % ss; Form III%: % ds); (b) plots that depict all values derived from all (at least three) experiments for the same compounds. (Plots on the bottom in blue color: % ss; plots on the top in red color: % ds).

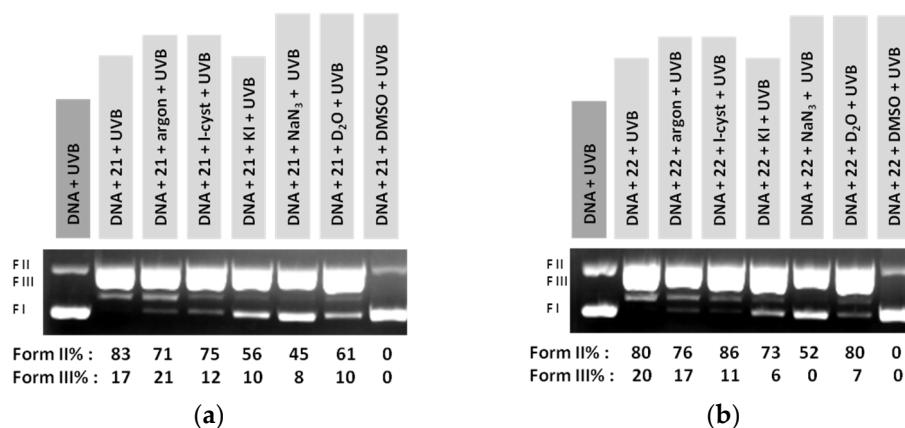


Figure 4. Gel electrophoresis pictures for the investigation of the mechanism of action in the presence of various scavengers: *L*-cyst: 1500 μ M; KI: 250 μ M; NaN₃: 20 mM; DMSO 20%. (a) Amidoxime carbamate **21**; (b) amidoxime carbamate **22**.

In air, a radical scavenger such as *L*-cyst does not influence the photocleavage, whereas KI decreased the activity. The same has been observed with excess NaN₃. In the presence of D₂O, the activity compared to the one in the presence of NaN₃ was increased, and this verifies the formation of singlet oxygen (type II mechanism [22]). Finally, the most drastic change was observed when excess DMSO was used. DMSO scavenges \cdot OH radicals, and this experiment indicated the formation of those radicals under the type I mechanism [22] (Figure 4).

Although derivatives **21–29** in DMSO solutions show low absorption in UVA areas above 350 nm (Supplementary Materials, Section S2A), their complexes with DNA seem to respond to those irradiations. Representatively, the UV-vis spectra of compounds **17**, **22**, **26**, and **28** with increasing amounts of CT-DNA have been recorded, and their K_b values have been calculated (Supplementary Materials, Section S2B and Table S1). According to the DNA-binding constants of the four studied derivatives, compound **17** showed the best affinity. The interaction with plasmid DNA and irradiation under a broad-band UVA lamp gave results similar to those obtained at 312 nm as far as the nature of the halogen atom concerns. Thus, for the 4-MeO-Ph derivatives, active were the F, Cl, and Br at the *p*-position (**22–24**). Derivative **21** was also found to be as active as **22** (Figure 5). All three *p*-, *m*-, and *o*-nitro-phenyl derivatives (**16–18**) were almost equally active, and hydrazone derivative **32**

showed some activity too (Figure 5 and Supplementary Materials Figure S3D. All gels are provided in Supplementary Materials, Section S4).

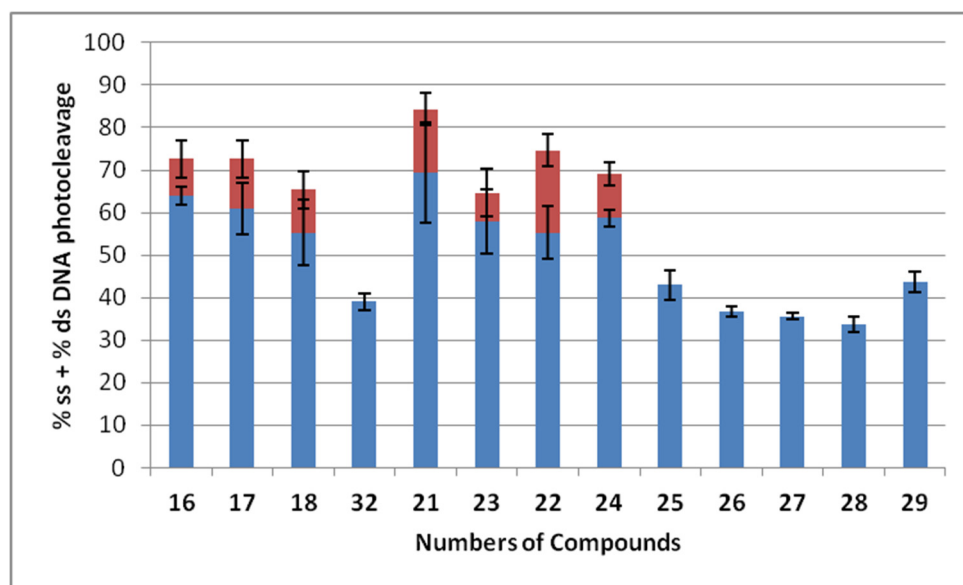


Figure 5. Plots that depict all values derived from all experiments for the same compounds, UV-A irradiation, 365 nm. (Plots on the bottom in blue color: % ss; plots on the top in red color: % ds).

The results of the DNA photocleavage provided the activity of the complexes that the compounds themselves form with DNA as a result of their affinity to the macromolecule. In order to expand studies to other molecules and/or organisms, one has to rely, initially, on the ability of the compounds to absorb light in the area of irradiation that is going to be used. Therefore, only derivatives **16–18** fulfill this prerequisite. Based on the fact that **16** and **17** were more easily obtained (**18** was obtained in a lower yield and required column chromatography purification) and their high UVA absorption, those two were selected for the pesticidal activity studies. Among those two compounds, compound **17** exhibited some activity, and the primitive results are presented below.

3.3. Pesticidal Activity

The effects of compound **17** have been evaluated against *B. tabaci*, a devastating crop pest all over the world. The mortality levels exhibited by **17** on whitefly nymphs were of low levels and were not affected by the 24 h exposure to UVA irradiation at 365 nm. The response of TYM 21-3 to **17** is shown in Figure 6. The corrected mortality for larvae of *B. tabaci* was 7% and 5.14% without and under UVA irradiation, respectively. Statistical analysis was performed (one-way ANOVA, $p > 0.05$, $n = 4$), indicating that the activation of compound **17** by UVA irradiation had no significant effects on the % mortality of whitefly nymphs. In contrast, the % mortality of adult whiteflies by **17** was 25% under UVA irradiation at 365 nm, whereas it was almost zero (0.2%) when **17** was inactive in the absence of UVA irradiation, suggesting that the activation of **17** was implicated in vital functions of the insect (one-way ANOVA indicated a significant increase in the % mortality levels under UVA irradiation ($p < 0.05$, $n = 3$), Figure 6).

This is not the first time that stage-specific differentiations to an insecticidal compound have been identified. Differences in response to xenobiotics in *B. tabaci* have been associated with genes that are differently expressed in different developmental stage. For example, resistance to the neonicotinoid insecticide imidacloprid can be detected in whitefly adults but not in the nymphal stages of individuals of the same population due to the stage-specific expression of P450s, metabolic enzymes associated with the resistance to neonicotinoids [61–63].

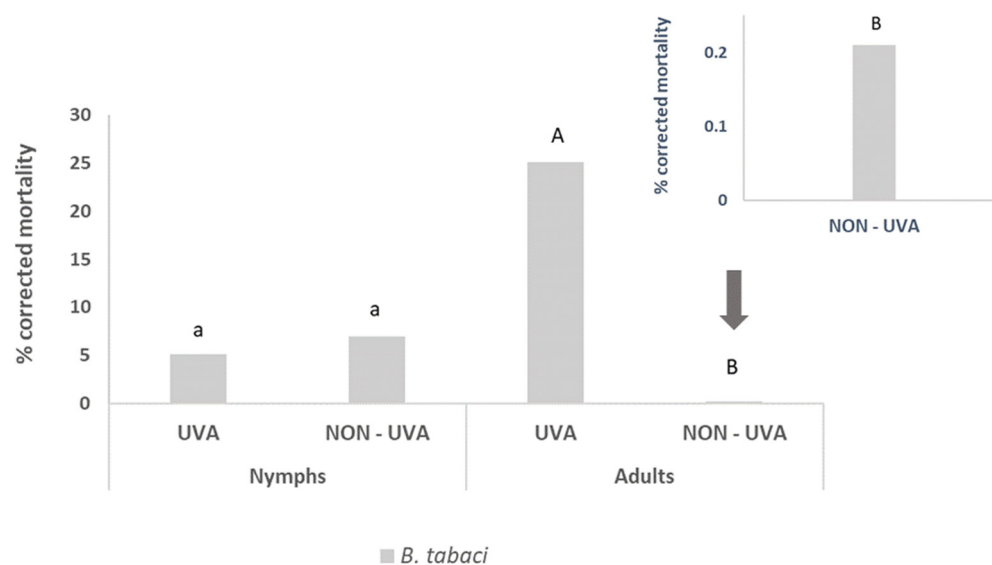


Figure 6. Estimated corrected mortality of L2 nymphs and adults of TYM 21-3 at dose 400 mgL⁻¹, under the exposure of 24 h of UVA irradiation at 365 nm and without UVA. Different Latin characters indicate significant differences in the responses ($p < 0.05$, one-way ANOVA, lowercase characters for nymph, and capital letters for adult comparisons).

The consequences of the implementation of compound **17** remain a knowledge gap. However, this is the first report on carbamates or oxime esters that act photochemically on insects. The results are preliminary but indicative of the direction that investigations on such applications should take. It could be further investigated for longer periods of exposure under UVA and/or visible light and evaluated on the population's development in a long term. Furthermore, for an assessment of the actions of this substance, more experiments using wider ranges of doses must be carried out in order to precisely define the optimal dose that could be potentially be used for the formulation of a novel insecticidal product.

4. Conclusions

A number of halogenated *O*-carbamoyl derivatives of 4-MeO-benzamidoxime derivatives have been designed in order to study their DNA photocleavage effect under UVB and UVA irradiation, with an emphasis on the nature, position, and number of halogens on the carbamoyl moiety that ensure photoactivity. After the efficient synthesis of all aryl carbamoyl esters bearing halogens in *p*-position (F, Cl, Br, and I), the most effective derivative towards DNA photocleavage was found to be the chlorinated one (**22**), in concentrations below 10 μ M. This result led to the investigation of the existence of the chlorine atom in other positions on the aryl moiety, meaning at the *m*- and *o*-position, as well as of the existence of two chlorine atoms on the aromatic ring that links the -NH-CO-O fragment. It was clear that the activity had been diminished not only at the *m*-chloro derivative (**26**) but also at the bis-chloro substituted ones (**28** and **29**). The substitution on the benzamidoxime scaffold seemed to be irrelevant to the outcome of the photocleavage. The ability of the compounds to react even in the absence of oxygen, probably via radicals derived from the N-O bond homolysis of the carbamates, is found to be important for the use of such compounds in hypoxic environments. Additionally, mechanistic studies for two compounds have shown that, in air, the formation of hydroxyl radicals and partially singlet oxygen is possible. The response of nitro-benzamidoxime *p*-Cl-PCMEs under UVA irradiation at 365 nm allowed for the investigation of their potential efficacy against the whitefly *B. tabaci*. The *m*-nitro derivative exhibited a moderate but significant specific activity against the adult stage of the pest only under UVA irradiation. Whitefly nymphs were not affected. This result, although very preliminary, may allow for the development of lead compounds

for the control of agricultural insect pests that can cause significant economic damage in crop production.

Supplementary Materials: The following supporting information can be downloaded at <https://www.mdpi.com/article/10.3390/dna3020006/s1>, Section S1A: Copies of NMR spectra of compounds **16–29** and **32**, Section S1B: Copies of HRMS measurements of compounds **16–29** and **32**, Section S2A: Copies of UV-vis spectra of compounds **16–29** and **32**, Section S2B: Copies of UV-vis spectra of compounds **17**, **22**, **26** and **28** upon increasing amounts of CT-DNA; Section S3: Gel electrophoresis pictures and plots, Figure S3A: Gel electrophoresis picture of the UVB irradiation of plasmid DNA with compounds **18–20**, Figure S3B: Concentration dependence of the DNA damage of compound **22**, Figure S3C: Gel electrophoresis picture of plasmid DNA with compounds **22–29** in the dark, Figure S3D: Gel electrophoresis picture of compounds **16–29** and **32** under UVA irradiation; Section S4: Gel electrophoresis pictures uncropped.

Author Contributions: Conceptualization, K.C.F.; methodology, E.R. and K.C.F.; validation, A.P., K.A., K.M., P.P., S.R., E.R. and K.C.F.; formal analysis, S.R., A.E.K., E.R. and K.C.F.; investigation, A.P., K.A., K.M. and P.P.; resources, A.E.K., E.R. and K.C.F.; data curation, A.E.K., E.R. and K.C.F.; writing—original draft preparation, K.C.F.; writing—review and editing, A.E.K., E.R. and K.C.F.; supervision, K.C.F.; project administration, K.C.F. All authors have read and agreed to the published version of the manuscript.

Funding: This research received no external funding.

Institutional Review Board Statement: Not applicable.

Informed Consent Statement: Not applicable.

Data Availability Statement: Not applicable.

Acknowledgments: K.C.F. and E.R. are grateful to Ekaterini Chatzaki, Director of the Institute of Agri-Food and Life Sciences Agro-Health, Hellenic Mediterranean University Research Center, for her efforts in establishing collaborations within the Institute. The authors also acknowledge technical support from Mikra Chryssoula. Special thanks to Maroula G. Kokotou, Laboratory of Chemistry, Department of Food Science and Human Nutrition, Agricultural University of Athens, for the HRMS analysis, and George Psomas for the calculation of K_b values.

Conflicts of Interest: The authors declare no conflict of interest.

References

1. McBurney, R.T.; Walton, J.C. Dissociation or Cyclization: Options for a Triad of Radicals Released from Oxime Carbamates. *J. Am. Chem. Soc.* **2013**, *135*, 7349–7354. [[CrossRef](#)] [[PubMed](#)]
2. Tsunooka, M.; Suyama, K.; Okamura, H.; Shirai, M. Development of Photoacid and Photobase Generators as the Key Materials for Design of Novel Photopolymers. *J. Photopolym. Sci. Technol.* **2006**, *19*, 65–71. [[CrossRef](#)]
3. Zheng, Y.; Yang, Y.; Yang, H.; Han, F.; Li, Z. Thioxanthone-Based Amidine: An Efficient Nonionic Photobase Generator for Thiol-Based Click Polymerization under Visible LED Light. *Prog. Org. Coat.* **2020**, *148*, 105842. [[CrossRef](#)]
4. Huang, L.; Xie, G.; Yang, J. A Fluorinated Photobase Generator with UVA Sensitive for Surface Oxygen Inhibition. *Prog. Org. Coat.* **2020**, *143*, 105604. [[CrossRef](#)]
5. Zhang, X.; Xi, W.; Gao, G.; Wang, X.; Stansbury, J.W.; Bowman, C.N. O-Nitrobenzyl-Based Photobase Generators: Efficient Photoinitiators for Visible-Light Induced Thiol-Michael Addition Photopolymerization. *ACS Macro Lett.* **2018**, *7*, 852–857. [[CrossRef](#)]
6. Terada, K.; Furutani, M.; Arimitsu, K. Development of Photobase Generators Liberating Radicals as Well as Bases and Their Application to Hardcoating Materials. *J. Photopolym. Sci. Technol.* **2018**, *31*, 493–496. [[CrossRef](#)]
7. Arimitsu, K.; Oguri, A.; Furutani, M. 365 Nm-Light-Sensitive Photobase Generators Derived from Trans-o-Coumaric Acid. *Mater. Lett.* **2015**, *140*, 92–94. [[CrossRef](#)]
8. Zivic, N.; Kuroishi, P.K.; Dumur, F.; Gimes, D.; Dove, A.P.; Sardon, H. Recent Advances and Challenges in the Design of Organic Photoacid and Photobase Generators for Polymerizations. *Angew. Chem. Int. Ed.* **2019**, *58*, 10410–10422. [[CrossRef](#)]
9. De Pariza, X.L.; Jara, E.C.; Zivic, N.; Rupiérrez, F.; Long, T.E.; Sardon, H. Novel Imino- and Aryl-Sulfonate Based Photoacid Generators for the Cationic Ring-Opening Polymerization of ϵ -Caprolactone. *Polym. Chem.* **2021**, *12*, 4035–4042. [[CrossRef](#)]
10. Lalevéé, J.; Allonas, X.; Fouassier, J.P.; Tachi, H.; Izumitani, A.; Shirai, M.; Tsunooka, M. Investigation of the Photochemical Properties of an Important Class of Photobase Generators: The O-Acyloximes. *J. Photochem. Photobiol. A Chem.* **2002**, *151*, 27–37. [[CrossRef](#)]

11. Walton, J.C. Functionalised Oximes: Emergent Precursors for Carbon-, Nitrogen- and Oxygen-Centred Radicals. *Molecules* **2016**, *21*, 63. [[CrossRef](#)]
12. Alonso, R.; Caballero, A.; Campos, P.J.; Rodríguez, M.A. Photochemistry of Acyloximes: Synthesis of Heterocycles and Natural Products. *Tetrahedron* **2010**, *66*, 8828–8831. [[CrossRef](#)]
13. Alonso, R.; Campos, P.J.; Rodríguez, M.A.; Sampedro, D. Photocyclization of Iminyl Radicals: Theoretical Study and Photochemical Aspects. *J. Org. Chem.* **2008**, *73*, 2234–2239. [[CrossRef](#)] [[PubMed](#)]
14. Van Der Westhuyzen, R.; Mabhula, A.; Njaria, P.M.; Müller, R.; Muhunga, D.N.; Taylor, D.; Lawrence, N.; Njoroge, M.; Brunschwig, C.; Moosa, A.; et al. Benzoheterocyclic Oxime Carbamates Active against Mycobacterium Tuberculosis: Synthesis, Structure-Activity Relationship, Metabolism, and Biology Triaging. *J. Med. Chem.* **2021**, *64*, 9444–9457. [[CrossRef](#)] [[PubMed](#)]
15. Keurulainen, L.; Heiskari, M.; Nenonen, S.; Nasereddin, A.; Kopelyanskiy, D.; Leino, T.O.; Yli-Kauhaluoma, J.; Jaffe, C.L.; Kiuru, P. Synthesis of Carboximidamide-Substituted Benzo[c][1,2,5]Oxadiazoles and Their Analogs, and Evaluation of Biological Activity against Leishmania Donovanii. *MedChemComm* **2015**, *6*, 1673–1678. [[CrossRef](#)]
16. Ke, S.; Yang, Z.; Shi, L.; Liu, M.; Liang, Y.; Wang, K.; Long, T.; Jiang, A.; Zhang, Z. Oxime Carbamates as Potential Insecticidal Agents: Design, Synthesis and Biological Evaluation. *Lett. Drug Des. Discov.* **2015**, *12*, 771–777. [[CrossRef](#)]
17. Sun, M.; Xu, W.; Zhang, W.; Guang, C.; Mu, W. Microbial Elimination of Carbamate Pesticides: Specific Strains and Promising Enzymes. *Appl. Microbiol. Biotechnol.* **2022**, *106*, 5973–5986. [[CrossRef](#)]
18. Malhotra, H.; Kaur, S.; Phale, P.S. Conserved Metabolic and Evolutionary Themes in Microbial Degradation of Carbamate Pesticides. *Front. Microbiol.* **2021**, *12*, 648868. [[CrossRef](#)]
19. Bhatt, P.; Zhou, X.; Huang, Y.; Zhang, W.; Chen, S. Characterization of the Role of Esterases in the Biodegradation of Organophosphate, Carbamate, and Pyrethroid Pesticides. *J. Hazard. Mater.* **2021**, *411*, 125026. [[CrossRef](#)]
20. Liu, Y.; Wang, X.; Nong, S.; Bai, Z.; Han, N.; Wu, Q.; Huang, Z.; Ding, J. Display of a Novel Carboxylesterase CarCby on Escherichia Coli Cell Surface for Carbaryl Pesticide Bioremediation. *Microb. Cell Factories* **2022**, *21*, 97. [[CrossRef](#)]
21. Moreira, S.; Silva, R.; Carrageta, D.F.; Alves, M.G.; Seco-Rovira, V.; Oliveira, P.F.; de Lourdes Pereira, M. Carbamate Pesticides: Shedding Light on Their Impact on the Male Reproductive System. *Int. J. Mol. Sci.* **2022**, *23*, 8206. [[CrossRef](#)]
22. Lima, A.R.; Dias, L.D.; Garbuio, M.; Inada, N.M.; Bagnato, V.S. A Look at Photodynamic Inactivation as a Tool for Pests and Vector-Borne Diseases Control. *Laser Phys. Lett.* **2022**, *19*, 025601. [[CrossRef](#)]
23. Ambrosini, V.; Issawi, M.; Sol, V.; Riou, C. Photodynamic Inactivation of Botrytis Cinerea by an Anionic Porphyrin: An Alternative Pest Management of Grapevine. *Sci. Rep.* **2020**, *10*, 17438. [[CrossRef](#)] [[PubMed](#)]
24. Losi, A.; Gärtner, W. A Light Life Together: Photosensing in the Plant Microbiota. *Photochem. Photobiol. Sci.* **2021**, *20*, 451–473. [[CrossRef](#)]
25. Stracke, F.; Heupel, M.; Thiel, E. Singlet Molecular Oxygen Photosensitized by Rhodamine Dyes: Correlation with Photophysical Properties of the Sensitizers. *J. Photochem. Photobiol. A Chem.* **1999**, *126*, 51–58. [[CrossRef](#)]
26. Jeon, R.; Wender, P.A. Photocleavage of DNA by 4'-Bromoacetophenone Analogs. *Arch. Pharmacol. Res.* **2001**, *24*, 39–43. [[CrossRef](#)] [[PubMed](#)]
27. Liu, D.; Yuan, G.; Hu, J. Synthesis and Photo-Induced DNA Cleaving Activities of Conjugates of Halophenyl Derivative and Polyamide Containing N-Methylimidazoles. *J. Photochem. Photobiol. B Biol.* **2006**, *82*, 187–193. [[CrossRef](#)] [[PubMed](#)]
28. Panagopoulos, A.; Balalas, T.; Mitrakas, A.; Vrazas, V.; Katsani, K.R.; Koumbis, A.E.; Koukourakis, M.I.; Litinas, K.E.; Fylaktakidou, K.C. 6-Nitro-Quinazolin-4(3H)-one Exhibits Photodynamic Effects and Photodegrades Human Melanoma Cell Lines. A Study on the Photoreactivity of Simple Quinazolin-4(3H)-ones. *Photochem. Photobiol.* **2021**, *97*, 826–836. [[CrossRef](#)]
29. Qian, X.; Yao, W.; Chen, G.; Huang, X.; Mao, P. N-Aroyloxynaphthalimides as Novel Highly Efficient DNA Photocleavers: Substituent Effects. *Tetrahedron Lett.* **2001**, *42*, 6175–6178. [[CrossRef](#)]
30. Chowdhury, N.; Dutta, S.; Dasgupta, S.; Singh, N.D.P.; Baidya, M.; Ghosh, S.K. Synthesis, Photophysical, Photochemical, DNA Cleavage/Binding and Cytotoxic Properties of Pyrene Oxime Ester Conjugates. *Photochem. Photobiol. Sci.* **2012**, *11*, 1239–1250. [[CrossRef](#)]
31. Hwu, J.R.; Tsay, S.C.; Hong, S.C.; Hsu, M.H.; Liu, C.F.; Chou, S.S.P. Relationship between Structure of Conjugated Oxime Esters and Their Ability to Cleave DNA. *Bioconjug. Chem.* **2013**, *24*, 1778–1783. [[CrossRef](#)]
32. Bindu, P.J.; Mahadevan, K.M.; Satyanarayan, N.D.; Naik, T.R.R. Synthesis and DNA Cleavage Studies of Novel Quinoline Oxime Esters. *Bioorganic Med. Chem. Lett.* **2012**, *22*, 898–900. [[CrossRef](#)] [[PubMed](#)]
33. Xu, Y.; Huang, X.; Qian, X.; Yao, W. N-Aroyloxylthioxo-Naphthalimides as DNA Photocleavers of Aroyloxyl Oxygen Radicals: Synthesis, Evaluation, and Substituents' Effect. *Bioorg. Med. Chem.* **2004**, *12*, 2335–2341. [[CrossRef](#)]
34. Karamtzioti, P.; Papastergiou, A.; Stefanakis, J.G.; Koumbis, A.E.; Anastasiou, I.; Koffa, M.; Fylaktakidou, K.C. O-Benzoyl Pyridine Aldoxime and Amidoxime Derivatives: Novel Efficient DNA Photo-Cleavage Agents. *MedChemComm* **2015**, *6*, 719–726. [[CrossRef](#)]
35. Pasolli, M.; Dafnopoulos, K.; Andreou, N.P.; Gritzapis, P.S.; Koffa, M.; Koumbis, A.E.; Psomas, G.; Fylaktakidou, K.C. Pyridine and P-Nitrophenyl Oxime Esters with Possible Photochemotherapeutic Activity: Synthesis, DNA Photocleavage and DNA Binding Studies. *Molecules* **2016**, *21*, 864. [[CrossRef](#)] [[PubMed](#)]

36. Andreou, N.P.; Dafnopoulos, K.; Tortopidis, C.; Koumbis, A.E.; Koffa, M.; Psomas, G.; Fylaktakidou, K.C. Alkyl and Aryl Sulfonyl P-Pyridine Ethanone Oximes Are Efficient DNA Photo-Cleavage Agents. *J. Photochem. Photobiol. B Biol.* **2016**, *158*, 30–38. [CrossRef]
37. Papastergiou, A.; Perontsis, S.; Gritzapis, P.; Koumbis, A.E.; Koffa, M.; Psomas, G.; Fylaktakidou, K.C. Evaluation of O-Alkyl and Aryl Sulfonyl Aromatic and Heteroaromatic Amidoximes as Novel Potent DNA Photo-Cleavers. *Photochem. Photobiol. Sci.* **2016**, *15*, 351–360. [CrossRef]
38. Gritzapis, P.S.; Varras, P.C.; Andreou, N.P.; Katsani, K.R.; Dafnopoulos, K.; Psomas, G.; Peitsinis, Z.V.; Koumbis, A.E.; Fylaktakidou, K.C. P-Pyridinyl Oxime Carbamates: Synthesis, DNA Binding, DNA Photocleaving Activity and Theoretical Photodegradation Studies. *Beilstein J. Org. Chem.* **2020**, *16*, 337–350. [CrossRef]
39. Siragusa, M.; Lentini, M.; Schepis, C. Agminated Lentiginosis in a Patient with Ring Chromosome 21. *Eur. J. Dermatol.* **2012**, *22*, 801–803. [CrossRef]
40. Lehmann, P. UV-B-Therapie von Hautkrankheiten: Ein Update Zu Indikationen, Wirksamkeit, Nebenwirkungen Und Durchführung. *Aktuelle Derm.* **2018**, *44*, 15–18, In German. [CrossRef]
41. Bala, H.R.; Khan, S.; Chong, A.H. Two Cases of Generalised Granuloma Annulare Successfully Treated with Acitretin and NB UVB Therapy. *Australas. J. Dermatol.* **2016**, *57*, 327–329. [CrossRef] [PubMed]
42. Zhou, J.; Yi, X.; Li, Y.; Ding, Y. Efficacy Assessment of UVA1 and Narrowband UVB for Treatment of Scalp Psoriasis. *Lasers Med. Sci.* **2018**, *33*, 1979–1982. [CrossRef] [PubMed]
43. Coricovac, D.; Farcas, C.; Nica, C.; Pinzaru, I.; Simu, S.; Stoian, D.; Soica, C.; Proks, M.; Avram, S.; Navolan, D.; et al. Ethinylestradiol and Levonorgestrel as Active Agents in Normal Skin, and Pathological Conditions Induced by UVB Exposure: In Vitro and in Ovo Assessments. *Int. J. Mol. Sci.* **2018**, *19*, 3600. [CrossRef] [PubMed]
44. Zabolinejad, N.; Maleki, M.; Salehi, M.; Ashrafi, Z.; Molkara, S.; Layegh, P. Psoralen and Narrowband UVB Combination Provides Higher Efficacy in Treating Vitiligo Compared with Narrowband UVB Alone: A Randomised Clinical Trial. *Australas. J. Dermatol.* **2020**, *61*, e65–e69. [CrossRef] [PubMed]
45. Al Salman, M.; Ghiasi, M.; Farid, A.S.; Taraz, M.; Azizpour, A.; Mahmoudi, H. Oral Simvastatin Combined with Narrowband UVB for the Treatment of Psoriasis: A Randomized Controlled Trial. *Dermatol. Ther.* **2021**, *34*, e15075. [CrossRef]
46. Ara, S.; Mowla, M.R.; Alam, M.; Khan, I. Efficacy of Oral Methotrexate (MTX) Monotherapy vs. Oral MTX plus Narrowband Ultraviolet Light B Phototherapy in Palmoplantar Psoriasis. *Dermatol. Ther.* **2020**, *33*, e13486. [CrossRef]
47. Martin, J.H.; Mifsud, D.; Rapisarda, C. The Whiteflies (Hemiptera: Aleyrodidae) of Europe and the Mediterranean Basin. *Bull. Entomol. Res.* **2000**, *90*, 407–448. [CrossRef]
48. Bedford, I.D.; Briddon, R.W.; Brown, J.K.; Rosell, R.C.; Markham, P.G. Geminivirus Transmission and Biological Characterisation of *Bemisia Tabaci* (Gennadius) Biotypes from Different Geographic Regions. *Ann. Appl. Biol.* **1994**, *125*, 311–325. [CrossRef]
49. Oliveira, M.R.V.; Anderson, P.; Oliveira, M.R.V.; Henneberry, T.J.; Anderson, P. History, Current Status, and Collaborative Research Projects for *Bemisia Tabaci*. *Crop Prot.* **2001**, *20*, 709–723. [CrossRef]
50. Roditakis, E.; Roditakis, N.E.; Tsagkarakou, A. Insecticide Resistance in *Bemisia Tabaci* (Homoptera: Aleyrodidae) Populations from Crete. *Pest Manag. Sci.* **2005**, *61*, 577–582. [CrossRef]
51. Sparks, T.C.; Nauen, R. IRAC: Mode of Action Classification and Insecticide Resistance Management. *Pestic. Biochem. Physiol.* **2015**, *121*, 122–128. [CrossRef]
52. Roditakis, E.; Grispou, M.; Morou, E.; Kristoffersen, J.B.; Roditakis, N.; Nauen, R.; Vontas, J.; Tsagkarakou, A. Current Status of Insecticide Resistance in Q Biotype *Bemisia Tabaci* Populations from Crete. *Pest Manag. Sci.* **2009**, *65*, 313–322. [CrossRef]
53. Bielza, P.; Moreno, I.; Belando, A.; Grávalos, C.; Izquierdo, J.; Nauen, R. Spiromesifen and Spirotetramat Resistance in Field Populations of *Bemisia Tabaci* Gennadius in Spain. *Pest Manag. Sci.* **2019**, *75*, 45–52. [CrossRef]
54. Horowitz, A.R.; Ghanim, M.; Roditakis, E.; Nauen, R.; Ishaaya, I. Insecticide Resistance and Its Management in *Bemisia Tabaci* Species. *J. Pest Sci.* **2020**, *93*, 893–910. [CrossRef]
55. Cai, J.; Wei, H.; Hong, K.H.; Wu, X.; Zong, X.; Cao, M.; Wang, P.; Li, L.; Sun, C.; Chen, B.; et al. Discovery, Bioactivity and Docking Simulation of Vorinostat Analogues Containing 1,2,4-Oxadiazole Moiety as Potent Histone Deacetylase Inhibitors and Antitumor Agents. *Bioorganic Med. Chem.* **2015**, *23*, 3457–3471. [CrossRef] [PubMed]
56. Vörös, A.; Mucsi, Z.; Baán, Z.; Timári, G.; Hermeicz, I.; Mizsey, P.; Finta, Z. An Experimental and Theoretical Study of Reaction Mechanisms between Nitriles and Hydroxylamine. *Org. Biomol. Chem.* **2014**, *12*, 8036–8047. [CrossRef] [PubMed]
57. Mettu, A.; Talla, V.; Bajaj, D.M.; Subhashini, N.J.P. Design, Synthesis, and Molecular Docking Studies of Novel Pyrazolyl 2-Aminopyrimidine Derivatives as HSP90 Inhibitors. *Arch. Pharm. Weinh.* **2019**, *352*, 1900063. [CrossRef] [PubMed]
58. IRAC Susceptibility Test Methods Series – Method No: 015. 2009. Available online: <https://irac-online.org/methods/trialeurodes-vaporariorum-bemisia-tabaci-adult/> (accessed on 31 March 2023).
59. IRAC Susceptibility Test Methods Series – Method No: 016. 2009. Available online: <https://irac-online.org/methods/trialeurodes-vaporariorum-bemisia-tabaci-nymphs/> (accessed on 31 March 2023).
60. Abbott, W.S. The Value of the Dry Substitutes for Liquid Lime. *J. Econ. Entomol.* **1925**, *18*, 265–267. [CrossRef]
61. Yang, N.; Xie, W.; Jones, C.M.; Bass, C.; Jiao, X.; Yang, X.; Liu, B.; Li, R.; Zhang, Y. Transcriptome Profiling of the Whitefly *Bemisia Tabaci* Reveals Stage-Specific Gene Expression Signatures for Thiamethoxam Resistance. *Insect Mol. Biol.* **2013**, *22*, 485–496. [CrossRef]

62. Nauen, R.; Bielza, P.; Denholm, I.; Gorman, K. Age-Specific Expression of Resistance to a Neonicotinoid Insecticide in the Whitefly *Bemisia Tabaci*. *Pest Manag. Sci.* **2008**, *63*, 1100–1106. [[CrossRef](#)]
63. Jones, C.M.; Daniels, M.; Andrews, M.; Slater, R.; Lind, R.J.; Gorman, K.; Williamson, M.S.; Denholm, I. Age-Specific Expression of a P450 Monooxygenase (CYP6CM1) Correlates with Neonicotinoid Resistance in *Bemisia Tabaci*. *Pestic. Biochem. Physiol.* **2011**, *101*, 53–58. [[CrossRef](#)]

Disclaimer/Publisher’s Note: The statements, opinions and data contained in all publications are solely those of the individual author(s) and contributor(s) and not of MDPI and/or the editor(s). MDPI and/or the editor(s) disclaim responsibility for any injury to people or property resulting from any ideas, methods, instructions or products referred to in the content.